

Article

Model Predictive Control of Uninterruptible Power Supply with Robust Disturbance Observer

Yahya Danaiyien ¹, Kyungsuk Lee ², Minho Choi ² and Young Il Lee ^{2,*}

¹ Department of Electrical and Electronics Engineering, Karadeniz Technical University, Trabzon 61080, Turkey

² Department of Electrical and Information Engineering, RCEIT, Seoul National University of Science and Technology, Seoul 01811, Korea

* Correspondence: yilee@seoultech.ac.kr; Tel.: +82-02-970-6544

Received: 13 June 2019; Accepted: 23 July 2019; Published: 25 July 2019



Abstract: This paper presents a robust continuous control set model predictive control (CCS-MPC) method to control the output voltage of a three-phase inverter in uninterruptible power supplies (UPS). A robust disturbance observer (DOB) is proposed to estimate the load current of the three-phase UPS without a steady-state error, taking the effect of model uncertainties into account. A CCS-MPC is designed using the DOB for reference voltage tracking purpose, and input constraints are considered in the controller design to calculate the optimal control input. Model uncertainties are defined using polytopic uncertainty class, and a linear matrix inequality (LMI) optimization method is used to compute the optimal observer gain matrix. Another robust controller (RC) is designed based on the DOB and compared with CCS-MPC. The effectiveness of the proposed method (the DOB based CCS-MPC) is evaluated for resistive, inductive, and nonlinear loads then compared with other control methods using a three-phase 5-KVA laboratory experiment UPS system.

Keywords: model predictive control (MPC), robust disturbance observer; optimal voltage control; three-phase inverter; uninterruptible power supplies (UPS)

1. Introduction

The main control objective for an uninterruptible power supply (UPS) is to regulate the output voltage in presence of parameter uncertainties and disturbances. The characteristic of a UPS is measured with its output voltage quality. The disturbances caused by various loads, such as inductive, nonlinear loads, and uncertainties caused by model mismatch lead to a lower tracking performance and high total harmonic distortion (THD) in the output voltage. The effect of the disturbances and uncertainties should be decreased to obtain a good voltage tracking performance [1]. Accordingly, control methods, such as deadbeat control [1,2], repetitive control [3,4], robust control [5–8], and model predictive control [9–15], have been used in conjunction with different observers to solve the aforementioned problems.

The deadbeat control method combined with state and disturbance observers, was successfully applied to a single-phase UPS inverter to compensate for the model uncertainties and load current disturbances [1]. A parameter estimation method with a deadbeat controller [2] can compensate for the white noise caused by sensed variables. However, this method requires a high sampling frequency, and is vulnerable to plant-model mismatch. The repetitive control method can provide satisfactory performances in the case of periodic errors if the internal model of the system is well defined [3,4]. However, this method is highly sensitive to parameter variation because of its dependence on the internal model and delays in the calculations. Other control methods, such as model reference control, can be included in the repetitive controller design to provide satisfactory performances [5]. Therefore, the resulting controller is complicated, and leads to a high computation burden during the implementation. Dissipativity-based adaptive robust control can eliminate the effects of parameter

uncertainties and load distortions with good voltage tracking performance in a UPS system [6]. Despite its fast-transient response and low THD, the resulting controller cannot compensate for the disturbances, and can yield a steady-state error in the presence of large parameter uncertainties and highly distorted loads.

In overcoming these problems, the model uncertainties can be defined as a polytopic uncertainty class [7], and controller gains can be calculated using the linear matrix inequality (LMI) method [7,8] for the purpose of robustness and optimality. A Luenberger-type observer is used in Reference [7] for the prediction of the system states. A robust controller is designed using the LMI method to control the output voltage of a UPS system. The output voltage THD is reasonable under nonlinear load, but is still high under linear loads. Moreover, the designed controller cannot be robust against a larger parameter variation.

Model predictive control has also been widely applied to the power converters in the last decade [9–15]. It can efficiently handle physical constraints and yields good performances. One of the main drawbacks of MPC is the steady-state offset error possibly caused by the prediction error, due to model uncertainties and disturbances. An integrator can be included in the MPC design to remove the offset error. In the UPS system, the lumped disturbances (model uncertainties and disturbance effect of the load current) can cause an offset error. Different kinds of disturbance observer (DOBs) were used with MPC, such as the Luenberger, Kalman filter types, etc., to compensate for these lumped disturbances and improve the close loop system performance [12–15]. A Luenberger-type disturbance observer was adopted in References [12,13] to compensate for the lumped disturbances in conjunction with the finite control set model predictive control (FCS-MPC) and the continuous control set model predictive control (CCS-MPC), respectively. Robust performance with a fast-transient response can be obtained with these methods; however, the offset error cannot be precisely removed because an integrator is not included in the DOB design [12,13], and the output voltage THD can be high [13]. A combined version of FCS-MPC and CCS-MPC was used with two different observers to remove the offset error and reduce the THD in the output voltage on the three-phase UPS system [14]. The first observer was a Luenberger-type observer used to compute the reference states. The second one was a disturbance observer designed to compensate for the lumped disturbances, including parameter uncertainties and noise. The output voltage THD was successfully reduced; however, a high sampling frequency was required, and an offset error existed in the output voltage.

An observer-based CCS-MPC method was suggested in Reference [15] for the purpose of the output voltage control of a UPS. A disturbance observer was designed to compensate for the effects of uncertainties and compute the reference states. The proposed method was successfully applied to the UPS system, and a stability analysis of the closed-loop system was well defined. However, a higher output THD was obtained under resistive and inductive loads, and the effectiveness of the method was not investigated under the nonlinear load. Moreover, the uncertainties were not well defined.

The disturbance observer based control methods have been applied to some other areas. A frequency domain disturbance observer was designed to remove the effect of the uncertainties in an induction motor application in Reference [16]. A disturbance observer was proposed for nonlinear systems in Reference [17] for DC motor control in Reference [18] and for robot system in Reference [19] to compensate the uncertainties in the systems.

Based on these observations in power converter systems and the MPC design mentioned earlier, a discrete time robust disturbance observer (DOB)-based CCS-MPC method is proposed for the purpose of the output voltage control of a UPS. The lumped disturbances caused by the model uncertainties and the load current are estimated by the proposed DOB. The DOB contains an integrator and enables the precise prediction of states in a steady state, despite the uncertainties. Thus, offset errors can be removed when this DOB is used in conjunction with CCS-MPC for the purpose of state tracking control. In earlier works [12–14], multiple disturbance observers, including Luenberger type observer were used in order to estimate the load current and model uncertainties, respectively to control the

UPS output voltage. In this approach, however, the use of only one disturbance observer is made to estimate the lumped disturbances, including the effect of load current and model uncertainties.

The control system is designed in the d–q reference frame, and the control signal is implemented using the SVPWM method. An LMI matrix is defined with an optimization problem to compute the observer gain matrix. The effectiveness of the control system is evaluated in a three-phase UPS system and compared to the robust control method [7], which is based on a Luenberger-type observer for resistive, inductive, and nonlinear loads for different uncertainty ranges.

The remainder of this paper is structured as follows: Section 2 describes the three-phase UPS system and modeling of uncertainties; Section 3 introduces a robust discrete time disturbance observer and shows an LMI method to find the observer gain matrix; Section 4 describes the control objective and provides the CCS-MPC design procedures; Section 5 provides the simulation and experimental results following by conclusion in Section 6.

2. System Description

2.1. Dynamic Model of the UPS

Figure 1 shows a three-phase two-level inverter with an output LC filter used in the UPS system. An unknown load that can be linear or nonlinear is connected to the filter output.

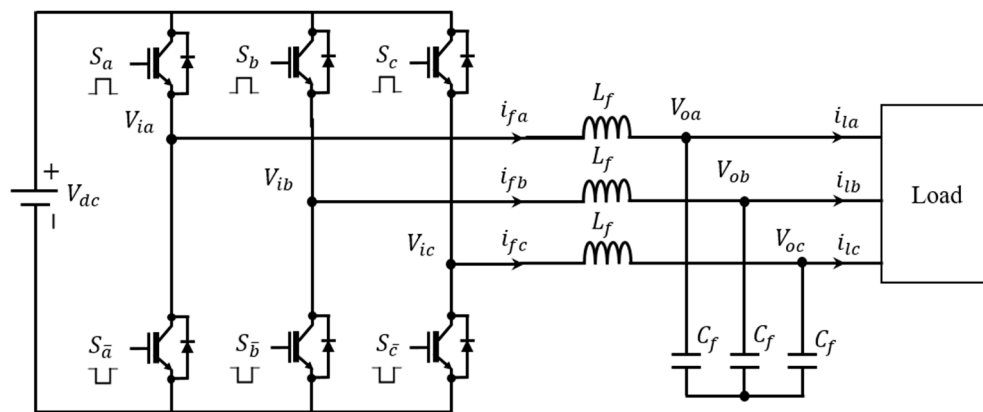


Figure 1. Three-phase inverter with LC filter.

Applying Kirchhoff's law, the filter dynamics can be obtained using three-phase quantities, as follows [7,20,21]:

$$\frac{di_f^{abc}(t)}{dt} = \frac{V_i^{abc}(t) - V_o^{abc}(t)}{L_f}, \quad (1)$$

$$\frac{dV_o^{abc}(t)}{dt} = \frac{i_f^{abc}(t) - i_l^{abc}(t)}{C_f}, \quad (2)$$

where $V_i^{abc}(t) = (V_{ia}, V_{ib}, V_{ic})$, $V_o^{abc}(t) = (V_{oa}, V_{ob}, V_{oc})$, $i_f^{abc}(t) = (i_{fa}, i_{fb}, i_{fc})$, and $i_l^{abc}(t) = (i_{la}, i_{lb}, i_{lc})$ are the vectors of the filter input voltage, output voltage (capacitor voltage), filter, and load currents, respectively. The input voltages can be defined using a switching function U_h ($h = a, b, c$) as:

$$V_i^{abc}(t) = \begin{bmatrix} V_{ia}(t) \\ V_{ib}(t) \\ V_{ic}(t) \end{bmatrix} = V_{dc} \begin{bmatrix} \frac{2}{3} & -\frac{1}{3} & -\frac{1}{3} \\ -\frac{1}{3} & \frac{2}{3} & -\frac{1}{3} \\ -\frac{1}{3} & -\frac{1}{3} & \frac{2}{3} \end{bmatrix} \begin{bmatrix} U_a \\ U_b \\ U_c \end{bmatrix}, \quad (3)$$

where

$$U_h = \begin{cases} 1, S_h = \text{ON}; S_{\bar{h}} = \text{OFF} \\ 0, S_h = \text{OFF}; S_{\bar{h}} = \text{ON} \end{cases} \quad (h = a, b, c \text{ and } \bar{h} = \bar{a}, \bar{b}, \bar{c}). \quad (4)$$

The two switches of an inverter leg are operated in a complementary mode to prevent short circuit of V_{dc} in the same leg.

The three-phase quantities in Equations (1) and (2) can be transformed into the rotating d-q frame using Park's transformation as follows:

$$\frac{di_f^{dq}(t)}{dt} = \omega M i_f^{dq}(t) + \frac{V_i^{dq}(t)}{L_f} - \frac{V_o^{dq}(t)}{L_f}, \quad (5)$$

$$\frac{dV_o^{dq}(t)}{dt} = \omega M V_o^{dq}(t) + \frac{i_f^{dq}(t)}{C_f} - \frac{i_l^{dq}(t)}{C_f}, \quad (6)$$

where $i_f^{dq}(t) = \begin{bmatrix} i_{fd}(t) \\ i_{fq}(t) \end{bmatrix} = T_{td}(\omega t) i_f^{abc}(t)$, $V_o^{dq}(t) = \begin{bmatrix} V_{od}(t) \\ V_{oq}(t) \end{bmatrix} = T_{td}(\omega t) V_o^{abc}(t)$,

$V_i^{dq}(t) = \begin{bmatrix} V_{id}(t) \\ V_{iq}(t) \end{bmatrix} = T_{td}(\omega t) V_i^{abc}(t)$, $i_l^{dq}(t) = \begin{bmatrix} i_{ld}(t) \\ i_{lq}(t) \end{bmatrix} = T_{td}(\omega t) i_l^{abc}(t)$,

$$M = \begin{bmatrix} 0 & 1 \\ -1 & 0 \end{bmatrix}, T_{td}(\omega t) = \frac{2}{3} \begin{bmatrix} \cos \omega t & \cos(\omega t - \frac{2}{3}\pi) & \cos(\omega t + \frac{2}{3}\pi) \\ -\sin \omega t & -\sin(\omega t - \frac{2}{3}\pi) & -\sin(\omega t + \frac{2}{3}\pi) \end{bmatrix}.$$

$T_{td}(\omega t)$, $\omega = 2\pi f_s$ and f_s are the transformation matrix, the angular frequency and the main frequency, respectively. The state space representation of Equations (5) and (6) in continuous time can be defined as

$$\frac{dx(t)}{dt} = A_c x(t) + B_c u(t) + W_c i_l^{dq}(t), \quad (7)$$

where $A_c = \begin{bmatrix} \omega M & -\frac{1}{L_f} I \\ \frac{1}{C_f} I & \omega M \end{bmatrix}$, $B_c = \begin{bmatrix} \frac{1}{L_f} I \\ 0_{2 \times 2} \end{bmatrix}$, $W_c = \begin{bmatrix} 0_{2 \times 2} \\ -\frac{1}{C_f} I \end{bmatrix}$, $u(t) = V_i^{dq}(t) = \begin{bmatrix} V_{id}(t) \\ V_{iq}(t) \end{bmatrix}$, $I \in \mathbb{R}^{2 \times 2}$ is an identity matrix, $0_{2 \times 2} \in \mathbb{R}^{2 \times 2}$ is a zero matrix, C_f and L_f are the filter capacitor and inductor, respectively.

The continuous time dynamics should be discretized to design an MPC. Here, with the assumption of a constant load current during the sampling period T_s , the discrete model of Equation (7) is obtained using Euler forward approximation [22] as follows:

$$x(k+1) = A_n x(k) + B_n u(k) + W_n i_l(k), \quad (8)$$

where $A_n \in \mathbb{R}^{4 \times 4} = e^{A_c T_s}$, $B_n \in \mathbb{R}^{4 \times 2} = \int_0^{T_s} e^{A_c t} B_c dt$, $W_n \in \mathbb{R}^{4 \times 2} = \int_0^{T_s} e^{A_c t} W_c dt$, $u(k) = \begin{bmatrix} u_d(k) \\ u_q(k) \end{bmatrix}$,

$x(k) = [i_{fd}(k) i_{fq}(k) V_{od}(k) V_{oq}(k)]^T$, $i_l^{dq}(k) = \begin{bmatrix} i_{ld}(k) \\ i_{lq}(k) \end{bmatrix}$. $u(k)$ and $x(k)$ are the vectors of the control input,

and system state, T denotes transpose of a vector or a matrix. $V_o^{dq}(k) = \begin{bmatrix} V_{od}(k) \\ V_{oq}(k) \end{bmatrix}$ is the output voltage vector to be controlled.

2.2. Modeling of Uncertainties

The resistive part of the three-phase load is assumed to be dominant, and i_o is considered to be a disturbance signal. The current source can be considered as a disturbance source for the filter, and the disturbance part of the load current is $i_o(t) = \frac{V_o^{dq}(t)}{R}$, as shown in Figure 2 [7]. With this disturbance term, Equation (8) can be rewritten as follows:

$$\frac{dx(t)}{dt} = \hat{A}_c x(t) + \hat{B}_c u(t) + W_c i_o^{dq}(t), \quad (9)$$

where $\hat{A} \in \mathbb{R}^{4 \times 4} = \begin{bmatrix} wM & -\frac{1}{L_f}I_u \\ -\frac{1}{C_f}I_u & wM - \frac{1}{RC_f}I_u \end{bmatrix}$, $I_u \in \mathbb{R}^{4 \times 4}$ is an identity matrix.

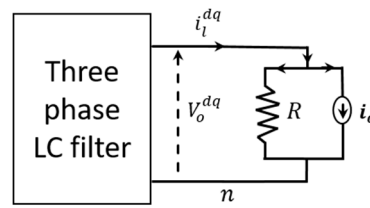


Figure 2. Uncertain load model.

It is assumed that the disturbance current $i_o(t)$ is constant during the sampling period T_s , Equation (9) can be discretized as

$$x(k+1) = \hat{A}x(k) + \hat{B}u(k) + W_n i_o(k), \tag{10}$$

where $\hat{A} \in \mathbb{R}^{4 \times 4} = e^{\hat{A}_c T_s}$, $\hat{B} \in \mathbb{R}^{4 \times 2} = \int_0^{T_s} e^{\hat{A}_c t} \hat{B}_c$, $W_n \in \mathbb{R}^{4 \times 2} = \int_0^{T_s} e^{\hat{A}_c t} W_c$

It is supposed that the three-phase parameters (resistors, inductors and capacitors) are equal and the load resistance R , the filter parameters L_f and C_f are uncertain, but have some values within a certain ranges, $R_1 \leq R \leq R_2$, $L_1 \leq L_f \leq L_2$, $C_1 \leq C_f \leq C_2$. The uncertain matrices (\hat{A} and \hat{B}) have ranges between the lower bounds (R_1, L_1, C_1) and the upper bounds (R_2, L_2, C_2) of the parameters. Assume that the matrix pairs (\hat{A}, \hat{B}) belongs a polytopic uncertain class \mathcal{P} [7]:

$$\mathcal{P} = \left\{ (\hat{A}, \hat{B}) \sum_{i=1}^p \gamma_i (A_i, B_i) \mid \sum_{i=1}^p \gamma_i = 1, \gamma_i \geq 0 \right\} \tag{11}$$

where \mathcal{P} is the polytopic uncertain class; γ is the increment of the parameter; and p is a positive integer ($i = 1, 2, \dots, p$ and $p = 2^{n_p} = 8$, n_p is the number of uncertain parameters in the system, in this paper, these parameters are L_f, C_f , and R). i th (\hat{A}, \hat{B}) pair of matrices are different from each other, and these pairs compose a convex set, in which \hat{A} and \hat{B} matrices are located. The upper and lower bounds of the uncertain parameters can be defined using an uncertainty norm η as follows:

$$L_1 = L_f / \eta, C_1 = C_f / \eta, R_1 = R / \eta, L_2 = L_f \eta, C_2 = C_f \eta, R_2 = R \eta, \tag{12}$$

3. Disturbance Observer Design

3.1. Dynamics of the Disturbance Observer

The predictive control algorithm highly depends on a system model; hence, the disturbances, model mismatches, etc., should be properly estimated. In this section, a discrete time robust DOB is proposed to estimate the lumped disturbance, including the effects of parameter uncertainties and unknown disturbance load currents.

The uncertain system (10) can be rewritten using nominal matrices (A_n, B_n) as follows:

$$x(k+1) = A_n x(k) + B_n u(k) + d_L(k), \tag{13}$$

where $d_L(k) \in \mathbb{R}^{4 \times 1}$ represents the lumped disturbance vector represented as:

$$d_L(k) = \Delta A x(k) + \Delta B u(k) + d(k), \tag{14}$$

where $\Delta A x(k) + \Delta B u(k)$ corresponds the model uncertainties and $\Delta A \in \mathbb{R}^{4 \times 4} = \hat{A} - A_n$, $\Delta B \in \mathbb{R}^{4 \times 2} = \hat{B} - B_n$, $d(k) = W_n i_o(k)$ corresponds the disturbance effect of the load current.

A disturbance observer is designed to estimate the lumped disturbance vector $d_L(k)$ as follows:

$$\hat{d}_L(k) = \hat{d}_L(k-1) + L(x(k) - A_n x(k-1) - B_n u(k-1) - \hat{d}_L(k-1)), \quad (15)$$

where $\hat{d}_L(k) = [\hat{d}_{L1} \ \hat{d}_{L2} \ \hat{d}_{L3} \ \hat{d}_{L4}]^T \in \mathbb{R}^{4 \times 1}$ is the estimated lumped disturbance vector, and L is the diagonal observer gain matrix to be determined.

The estimated lumped disturbance vector $\hat{d}_L(k)$ can asymptotically converge to its actual value $d_L(k)$ if the observer gain matrix L is chosen, such that the error between the actual state and the predicted state in Equation (15) converges to zero in the steady state. Using a constant input u_0 yields steady-state x_0 and steady-state disturbances, and two different representations can be obtained from Equations (10) and (13) as follows:

$$x_0 = \hat{A}x_0 + \hat{B}u_0 + d, \quad (16)$$

and

$$x_0 = A_n x_0 + B_n u_0 + d_L. \quad (17)$$

It is assumed that there is no error between the actual value and nominal value in the steady state, and subtracting Equation (17) from Equation (16), we have:

$$\Delta A x_0 + \Delta B u_0 + d - d_L = 0. \quad (18)$$

Inserting the relation (18) into (15), we have:

$$\hat{d}_L(k) = \hat{d}_L(k-1) + L(\hat{A}x(k-1) + \hat{B}u(k-1) + d - \Delta A x_0 - \Delta B u_0 - d + d_L - A_n x(k-1) - B_n u(k-1) - \hat{d}_L(k-1)), \quad (19)$$

and if we assume the use of a constant control input u_0 , Equation (19) can be rewritten as

$$\hat{d}_L(k) = (I - L)\hat{d}_L(k-1) + L(\Delta A x_e(k-1) + d_L), \quad (20)$$

where $x_e(k-1) = x(k-1) - x_0$. Furthermore, subtracting Equation (16) from Equation (13) yields:

$$x_e(k) = \hat{A}x_e(k-1) + \hat{B}u_e(k-1), \quad (21)$$

where $u_e(k-1) = u(k-1) - u_0$. Note that Equations (20) and (21) are the dynamics of the disturbance observer (15) when it is applied to the system (13) with a constant input $u(k) = u_0$.

3.2. Calculation of L Using LMI

In this section, an LMI formulation to compute a stabilizing gain L of Equation (15) is derived. From Equations (20) and (21), we have:

$$\begin{bmatrix} \hat{d}_L(k) \\ x_e(k) \end{bmatrix} = \begin{bmatrix} (I-L) & L\Delta A \\ 0 & \hat{A} \end{bmatrix} \begin{bmatrix} \hat{d}_L(k-1) \\ x_e(k-1) \end{bmatrix} + \begin{bmatrix} L & 0 \\ 0 & \hat{B} \end{bmatrix} \begin{bmatrix} d_L \\ u_e \end{bmatrix}. \quad (22)$$

Let us now define a new state variable $z(k)$ for (22) to check the stability of its homogeneous response:

$$z(k) = \psi z(k-1), \quad (23)$$

where $z(k) = \begin{bmatrix} \hat{d}_L(k) \\ x_e(k) \end{bmatrix}$, $\psi = \begin{bmatrix} (I-L) & L\Delta A \\ 0 & \hat{A} \end{bmatrix}$.

To satisfy the asymptotic stability in Equation (23), L matrix should be properly chosen, such that the ψ matrix is Hurwitz. The problem, now, is how to find the L . We drive herein an LMI to obtain

a robust L in the presence of uncertainties. The stability of ψ is guaranteed if a positive definite matrix P_{obv} satisfying

$$P_{obv} - \psi^T P_{obv} \psi > 0 \tag{24}$$

exists. If we assume that P_{obv} is a block diagonal matrix, $P_{obv} = \begin{bmatrix} P_1 & 0 \\ 0 & P_2 \end{bmatrix}$, then, Equation (24) can be rewritten as:

$$\begin{bmatrix} P_1 & 0 \\ 0 & P_2 \end{bmatrix} - \begin{bmatrix} (I-L) & L\Delta A \\ 0 & \hat{A} \end{bmatrix}^T \begin{bmatrix} P_1 & 0 \\ 0 & P_2 \end{bmatrix} \begin{bmatrix} (I-L) & L\Delta A \\ 0 & \hat{A} \end{bmatrix} > 0 \tag{25}$$

Relation (25) can be transformed into the following LMI using the Schur complement [19]:

$$\begin{bmatrix} \begin{bmatrix} P_1 & 0 \\ 0 & Q_2 \end{bmatrix} & \begin{bmatrix} (P_1 - Y) & Y\Delta A \\ 0 & \hat{A}Q_2 \end{bmatrix}^T \\ \begin{bmatrix} (P_1 - Y) & Y\Delta A \\ 0 & \hat{A}Q_2 \end{bmatrix} & \begin{bmatrix} P_1 & 0 \\ 0 & Q_2 \end{bmatrix} \end{bmatrix} > 0, \tag{26}$$

where $Y = P_1 L$. (26) should be checked for all uncertain matrices; hence, the system matrices can be any pair of matrices defined in the uncertain polytopic class. In the UPS system, there are $2^{n_p=3} = 8$ possible (\hat{A}, \hat{B}) pairs, which are vertices of \mathcal{P} . The LMI problem defined in Equation (26) can be rewritten as:

$$\begin{bmatrix} \begin{bmatrix} P_1 & 0 \\ 0 & Q_2 \end{bmatrix} & \begin{bmatrix} (P_1 - Y) & Y\Delta A_i \\ 0 & \hat{A}_i Q_2 \end{bmatrix}^T \\ \begin{bmatrix} (P_1 - Y) & Y\Delta A_i \\ 0 & \hat{A}_i Q_2 \end{bmatrix} & \begin{bmatrix} P_1 & 0 \\ 0 & Q_2 \end{bmatrix} \end{bmatrix} > 0, \tag{27}$$

where $i = 1, 2, \dots, 8$. Note that the solution of Equation (27) is not unique. An optimization criterion is defined to find an optimal solution of Equation (27) that can be calculated by reducing the Lyapunov function $V(k) = z(k)^T G z(k)$ as fast as possible if G_0 is reduced for a given G .

Suppose that

$$G < \varepsilon G_0, \tag{28}$$

where G_0 and G are positive definite symmetric matrices, and $0 < \varepsilon < 1$, ε can be considered as settling time. A small ε would yield a fast convergence rate of $V(k)$ [7]. Finally, the following problem can be solved to find an optimal G_0, G, L by minimizing ε .

$$\min_{\substack{\gamma \\ G, G_0 > 0 \\ \varepsilon, L}} \gamma \text{ subject to Equations (27) and (28)}. \tag{29}$$

4. Controller Design

4.1. CCS-MPC

In this section, CCS-MPC is derived for the reference voltage tracking problem based on the proposed DOB. The control objective can be represented as a state tracking problem:

$$\lim_{k \rightarrow \infty} x(k) = x^*(k), \tag{30}$$

where $x(k) = [i_{fd} \ i_{fq} \ V_d \ V_q]^T \in \mathbb{R}^{4 \times 1}$ is the state vector, and $x^*(k) = [i_{fd}^* \ i_{fq}^* \ V_d^* \ V_q^*]^T \in \mathbb{R}^{4 \times 1}$ is the reference state vector (Super script * denotes the reference values.). Note that the voltage references are

given as V_d^* and $V_q^* = 0$. Corresponding to these voltage references, consider the following steady-state condition to derive the current references and nominal control inputs:

$$x^*(k) = A_n x^*(k) + B_n u_0(k) + d_L(k), \quad (31)$$

and Equation (31) can be rewritten based on the estimated disturbance vector $\hat{d}_L(k)$ as:

$$x^*(k) = A_n x^*(k) + B_n u_0(k) + \hat{d}_L(k) \quad (32)$$

For the given voltage references, V_d^* and $V_q^* = 0$, reference filter currents, i_{fd}^* and i_{fq}^* , can be computed as follows:

$$i_{fd}^*(k) = \frac{V_d^*}{R} - \frac{C_f}{T_s} \hat{d}_{L3}(k), \quad (33)$$

$$i_{fq}^*(k) = \omega C_f V_d^* - \frac{C_f}{T_s} \hat{d}_{L4}(k), \quad (34)$$

and the nominal input $u_o(k) = [u_{od}(k) \ u_{oq}(k)]^T$ satisfying Equation (32) can be derived as:

$$u_{od}(k) = V_d^* - \omega L_f i_{fq}^* - \frac{L_f}{T_s} \hat{d}_{L1}(k), \quad (35)$$

$$u_{oq}(k) = \omega L_f i_{fd}^* - \frac{L_f}{T_s} \hat{d}_{L2}(k). \quad (36)$$

The prediction model of the system can be defined using nominal system matrices and $\hat{d}_L(k)$ as:

$$x(k+1|k) = A_n x(k) + B_n u(k) + \hat{d}_L(k), \quad (37)$$

where $x(k) \in \mathbb{R}^{4 \times 1}$ is the current state and $x(k+1|k) \in \mathbb{R}^{4 \times 1}$ is the predicted state calculated at time instant k . The predicted error is defined as:

$$e(k+1) = x(k+1|k) - x^*(k). \quad (38)$$

An optimization problem is defined in order to minimize the error system (38) and penalize the control input as:

$$\min_{u(k)} J(x(k), u(k)), \quad (39)$$

and the cost function is:

$$J(x(k), u(k)) = (e(k+1))^T P_{cost} (e(k+1)) + (u(k) - u_o(k))^T \bar{R} (u(k) - u_o(k)) \quad (40)$$

where $\bar{R} = r I_u^{2 \times 2}$; $I_u^{2 \times 2}$ is the unity matrix; r is the design parameter for penalizing the control input; and P_{cost} is a positive definite symmetric matrix with an optimal value that can be calculated using the LMI method considering the polytopic uncertain class (11) to make $J(k)$ of Equation (40) monotonically decreases (i.e., $J(k) - J(k+1) > 0$) when $u(k) = u_o(k)$). The following error dynamics can be obtained by subtracting Equation (32) from Equation (37):

$$e(k+1) = A_n e(k) + B_n \Delta u(k), \quad (41)$$

where $e(k) = x(k) - x^*(k)$, $\Delta u(k) = u(k) - u_o(k)$, and we obtain the following from Equations (40) and (41):

$$J(k) - J(k+1) = e(k)^T (P_{cost} - A_n^T P A_n) e(k) > 0 \quad (42)$$

(42) is guaranteed to be satisfied if:

$$P_0 - A_n^T P_{cost} A_n > 0, \tag{43}$$

where P_{cost} and P_0 ($P_0 < P_{cost}$) are positive definite matrices. Schur complement [23] can be applied to (43) to yield the following LMI:

$$\begin{bmatrix} Q_0 & A_i^T \\ A_i & Q \end{bmatrix} > 0, Q_0 > Q, \tag{44}$$

where $Q_0 = P_0^{-1}$ and $Q = P_{cost}^{-1}$, and Equation (44) can be solved by following a similar method: Equations (24)–(29). Note that the control input $u(k)$ is constrained to belong to the following set:

$$S_i \{ u(k) \in \mathbb{R}^2 \mid u(k) \leq U_{max} \} \tag{45}$$

where S_i is the boundary input set, which denotes the linear modulation range of the space vector pulse width modulation (SVPWM) limited with $U_{max} = \frac{V_{dc}}{\sqrt{3}}$, which is the radius of the inner circle represented in Figure 3. This constraint can be represented as:

$$\sqrt{u_d^2 + u_q^2} \leq U_{max} = \frac{V_{dc}}{\sqrt{3}}. \tag{46}$$

The optimal value of the control input $u^*(k)$ for the unconstrained case is determined from the first derivative of $J(x(k), u(k))$ as follows:

$$u_{uc}^*(k) = - \frac{(B_n^T P_{cost})(A_n(x(k) - x^*(k)))}{(B_n^T P_{cost} B_n + \bar{R})} + u_o(k), \tag{47}$$

where $u_{uc}^*(k)$ is the optimal input for an unconstrained case, $u_o(k)$ is the corresponding steady-state input satisfying Equation (32). Note that Equation (47) is composed of the $u_o(k)$ obtained as Equations (35) and (36) and a correction term. However, this control input is only valid if $u_{uc}^*(k) \in S_i$. If $\|u_{uc}^*(k)\| > U_{max}$ (i.e., $u_{uc}^*(k) \notin S_i$), then Equation (47) cannot be used.

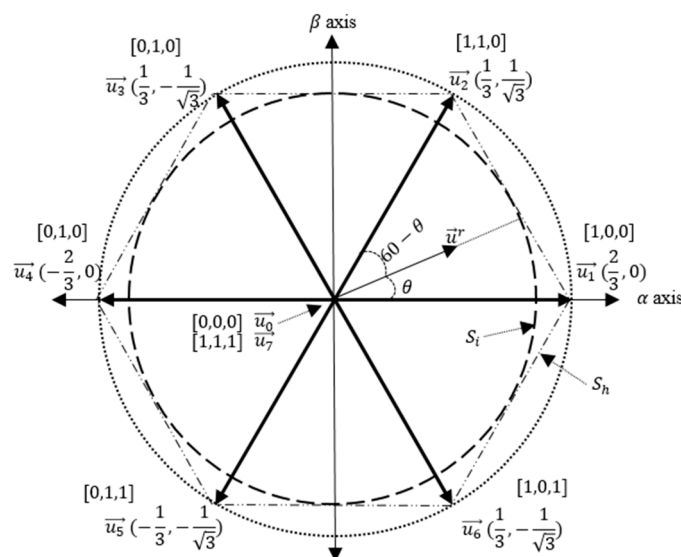


Figure 3. Voltage vectors and input constrained set.

In this case, u_{uc}^* should be modified, such that a feasible optimal solution can be obtained as [15]:

$$u^*(k) = \begin{cases} u_{uc}^*, & \text{if } u_{uc}^* \in S_i \\ \alpha u^*(k), & \text{if } u_{uc}^* \notin S_i \end{cases} \tag{48}$$

where $= \frac{V_{dc}}{\sqrt{3}\|u^*(k)\|}$. Note that (48) is valid if P_{cost} is obtained, such that $B^T P_{cost} B = \beta I$ for some positive scalar β [15].

Figure 4 shows the general block diagram of the controlled system. The currents $i_f^{abc}(k)$ and output voltages $V_o^{abc}(k)$ are measured then converted to the d-q reference frame using Park transformation. The disturbance observer (15) estimates $\hat{d}_L(k)$, and the estimated disturbance vector, $\hat{d}_L(k)$ is sent to the prediction and reference blocks. The error prediction (38) is then performed, and the optimal control input (48) is calculated and send to the SVPWM modulator.

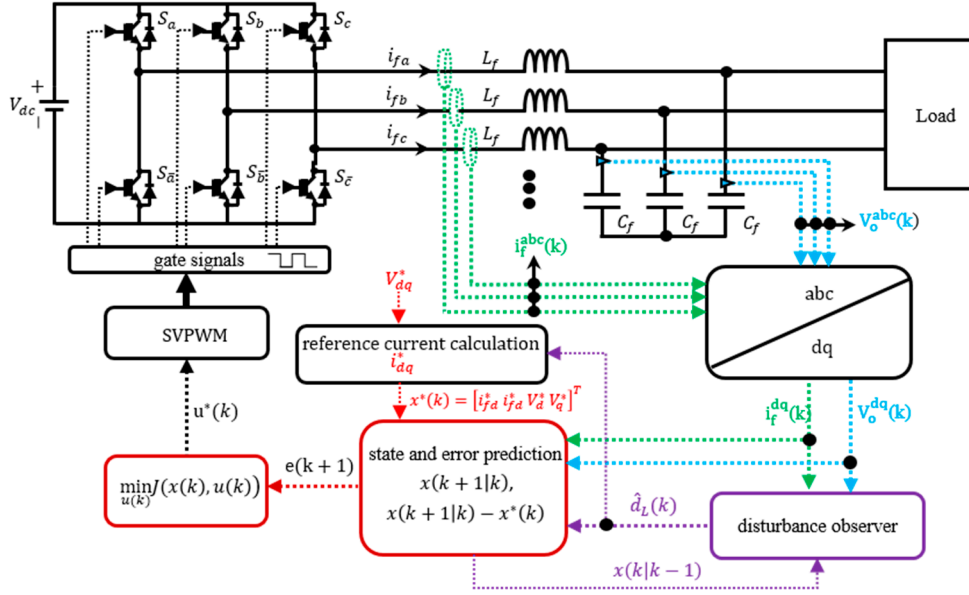


Figure 4. General block diagram of the system.

4.2. Compensation of the Input Time Delay

The use of an inverter will cause a one-step time delay (i.e., the control input $u(k)$ will actually be implemented at time step $k + 1$, and have an effect on $x(k + 2)$). Considering this input time delay, the disturbance observer (15) and the prediction model (37) should be rewritten as:

$$\hat{d}_L(k) = \hat{d}_L(k - 1) + L(x(k) - x(k|k - 1)), \tag{49}$$

$$x(k|k - 1) = A_n x(k - 1) + B_n u(k - 2) + \hat{d}_L(k - 1). \tag{50}$$

The cost index (40) should also be modified as

$$J(x(k), u(k)) = (e(k + 2|k))^T P_{cost} (e(k + 2|k)) + (u(k) - u_o(k))^T \bar{R} (u(k) - u_o(k)), \tag{51}$$

to yield the unconstrained control input

$$u^*(k) = - \frac{(B_n^T P_{cost}) A_n (x(k + 1|k) - x^*(k))}{(B_n^T P_{cost} B_n + \bar{R})} + u_o(k). \tag{52}$$

4.3. Robust Controller Design with the DOB (RC-DOB) and the Luenberger Type Observer (RC-LOB)

A robust controller (RC) is designed for the comparison purpose following [7] as

$$w(k + 1) = w(k) + (V_*^{dq} - V^{dq}(k)), \tag{53}$$

$$u(k) = K\hat{x}(k + 1|k) + Zw(k + 1), \tag{54}$$

where $V^{dq}(k) = [V_d \ V_q]^T$ and $V_*^{dq} = [V_d^* \ V_q^*]^T$ are the vectors of controlled output voltage and the reference voltage, K and Z are the feedback gain matrices. The one-step-ahead prediction $\hat{x}(k+1|k)$ could be made using the prediction model (37) for the robust controller with the proposed disturbance observer (RC-DOB) or using the robust controller with Luenberger type observer (RC-LOB) as in Reference [7]. Thus, we designed two control system to compare with the proposed method (DOB with CCS-MPC). The first control system is designed based on the proposed DOB, from Reference [7], and the abbreviation RC-DOB (robust controller with the proposed observer) will be used for it. The second one is a robust controller based on Luenberger type observer as in Reference [7], and the abbreviation RC-LOB will be used for it.

4.4. Stability Analysis

In this section, the stability analysis of the uncertain system and close loop system are given.

It is assumed that the filter parameters stay in the boundary range as in Equation (11). Based on this assumption, it can be said that the uncertain system (10) is stable for any parameter change within the range, and if a positive definite symmetric matrix $\hat{Q} = \hat{Q}^T > 0$ exists that satisfies

$$\hat{Q} - A_i^T \hat{Q} A_i > 0, \quad (55)$$

then, it is guaranteed that all uncertain system matrices (A_i) are stable. $\hat{Q} \in \mathbb{R}^{4 \times 4}$, $i = 1, 2, \dots, 8$, $A_i \in \mathcal{P}$. \mathcal{P} is the polytopic uncertainty class, which is defined in Equation (11). It means that, there are 8 number of \hat{A} matrices and all these matrices are stable, if the uncertain parameters (R, L_f, C_f) stay in the boundary range.

The close loop system matrix can be obtained using Equation (10) and observer dynamics (20) and (21) as follows:

$$\begin{bmatrix} \hat{d}_L(k) \\ x_e(k) \\ x(k+1) \end{bmatrix} = \begin{bmatrix} (I-L) & L\Delta A & 0 \\ 0 & \hat{A} & 0 \\ 0 & 0 & \hat{A} \end{bmatrix} \begin{bmatrix} \hat{d}_L(k-1) \\ x_e(k-1) \\ x(k) \end{bmatrix}, \quad (56)$$

and Equation (56) can be rewritten as

$$x_{cl}(k+1) = \hat{A}_{cl} x_{cl}(k). \quad (57)$$

where $x_{cl}(k+1) = [\hat{d}_L(k) \ x_e(k) \ x(k+1)]^T \in \mathbb{R}^{12 \times 1}$, $x_{cl} = [\hat{d}_L(k-1) \ x_e(k-1) \ x(k)]^T$, $\hat{A}_{cl} \in \mathbb{R}^{12 \times 12}$.

It is assumed that the observer gain matrix L is chosen such that the observer matrix ψ (23) is stable. Suppose that the weighting matrix P_{cost} of the cost function $J(x(k), u(k))$ satisfies the constraints $B^T P_{cost} B = \beta I$ (for some positive values of β , since $B^T P_{cost} B > 0$) and inequality (43) [15]. Based on the assumption, the close loop matrix \hat{A}_{cl} become stable, and therefore satisfies $P_{cl} = P_{cl}^T > 0$,

$$P_{cl} - \hat{A}_{cl}^T P_{cl} \hat{A}_{cl} > 0, \quad (58)$$

then, the close loop system (58) is globally asymptotically stable, the system state vector $x(k)$ and the estimated lumped disturbance vector $\hat{d}_L(k)$ converge to the reference state vector $x^*(k)$ and the actual disturbance vector $d_L(k)$ in the steady, which is

$$\lim_{k \rightarrow \infty} x(k) = x^*(k), \quad \lim_{k \rightarrow \infty} \hat{d}_L(k) = d_L(k), \quad (59)$$

where $k > 0$ and $\forall (x(k), \hat{d}_L(k)) \in \mathbb{R}^4$.

5. Results

5.1. Simulation Results

In this section, the comparative results are given in terms of the output voltage THD and transient response using the three different control methods (i.e., MPC-DOB, RC-DOB, and RC-LOB) in order to evaluate the performance of the proposed method. The optimal observer gain matrix L , K , Z and the gain matrix of the Luenberger type observer were calculated using MATLAB R2018a and YALMIP. The simulation model of the system was obtained in PSIM. The control algorithm was written in C programming language using Microsoft Visual Studio and implemented in PSIM using DLL block. The sampling period was set to be 10 kHz. The nominal filter parameters in Table 1 were used in the simulation.

Table 1. Nominal system parameters.

Parameter	Value
DC link voltage V_{dc}	230 V
Reference voltage V_d^*	110 V
Reference voltage V_q^*	0
Output frequency f_s	60 Hz
Sampling time T_s	100 μ s
Filter inductance L_f	1.3 mH
Filter capacitance C_f	50 μ F
Load resistance R	10 Ω

The effectiveness of the proposed method was verified under nonlinear, inductive and resistive load model given in Figure 5a–c, respectively. A three-phase diode rectifier was used as a nonlinear load and R_{nl} , C_{nl} , L_{nl} are the resistor, capacitor and inductor connected to the output of the nonlinear load, R_{LL} , L_{LL} are the inductive load resistor and inductor, R is the resistive load.

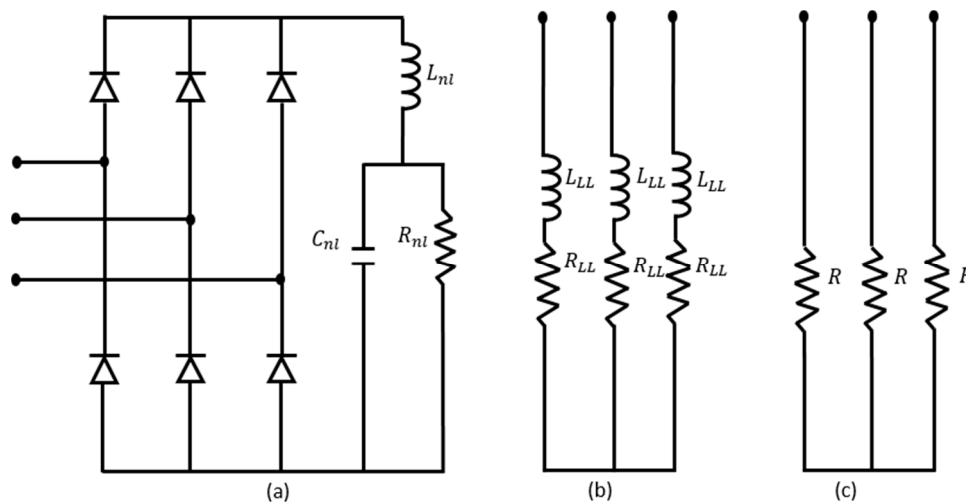


Figure 5. The three phases: (a) nonlinear, (b) inductive, and (c) resistive load models.

Firstly, the transient response of the CCS-MPC control input $u^*(k)$ of Equation (48) is verified to be better than that of the steady-state control input $u_o(k)$ of Equations (35) and (36), in case of a load change. Figure 6 shows that the transient behavior of the d-axis load current is slower, and a high oscillation exists with the control input $u_o(k)$ compared to $u^*(k)$ (CCS-MPC) under the resistive load ($R = 10 \Omega$) change at time step 1 s. $u_o(k)$ can not stabilize the system for large η values. Moreover, the THD values are reasonable (less than %3) for resistive load for both control inputs.

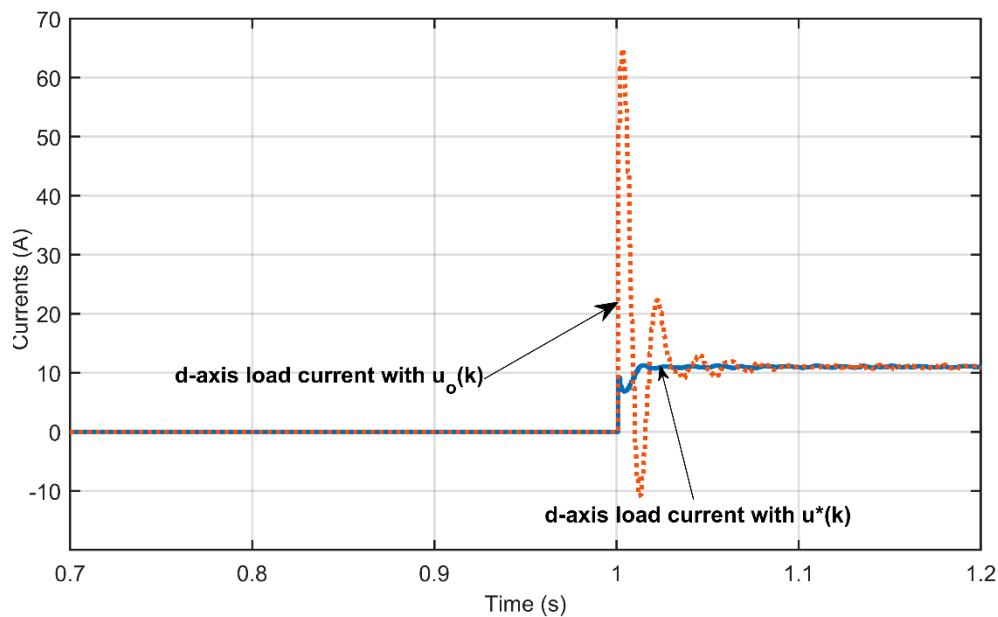


Figure 6. Transient behavior of the load current for the steady-state control input $u_o(k)$ and MPC control input $u^*(k)$ with $\eta = 3.5$ during the load change at time step 1 s ($THD = 1\%$ with $u^*(k)$, $THD = 2.2\%$ with $u_o(k)$, $R = 10 \Omega$).

Secondly, the transient response of the d-axis voltage is evaluated using the three control methods for $\eta = 7.5$. This value is chosen for a fair comparison, since the performance of the control methods are similar to each other for $\eta = 7.5$. Figure 7 indicates that a fast transient can be obtained using the proposed method (MPC-DOB) under the nonlinear load. The parameters are chosen as $R_{nl} = 200 \Omega$, $L_{nl} = 10$ mH and $C_{nl} = 2200 \mu\text{F}$. The result shows that the transient response of the d-axis voltage is faster when MPC-DOB is used, and slower, but more robust, when RC-DOB is used. Although a similar steady-state performance is obtained with RC-LOB and MPC-DOB in the steady state, a higher overshoot is obtained in the transient time with RC-LOB.

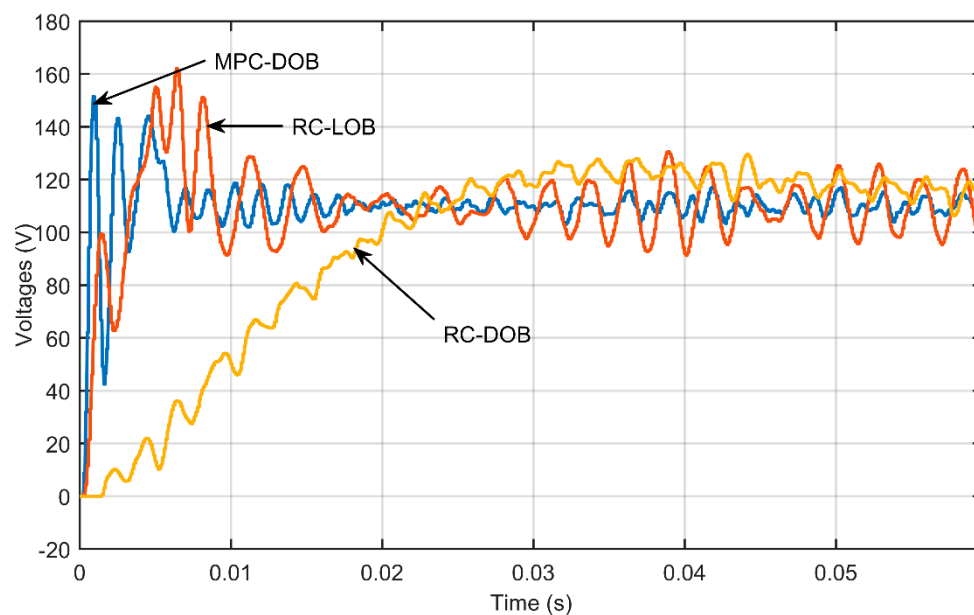


Figure 7. Transient response of the d-axis voltage with MPC-DOB, RC-DOB, and RC-LOB under the nonlinear load ($R_{nl} = 200 \Omega$, $L_{nl} = 10$ mH, $C_{nl} = 2200 \mu\text{F}$) for $\eta = 7.5$.

The effectiveness of the proposed method is verified for different uncertainty norm (η) values using the three methods under the nonlinear load. Table 2 shows the comparative results for output voltage THD values. It is verified that the lower THD can be obtained with MPC-DOB for large uncertainties ($\eta = 7.8$). The reasonable THD is obtained for $6.5 \leq \eta \leq 7.8$ with MPC-DOB, for $3.5 \leq \eta \leq 7.5$ with RC-DOB and RC-LOB. For some values of η , the closed-loop system becomes unstable, and the THD information is not available (NA in the tables).

Table 2. Comparison of the voltage THD values for different η under the nonlinear load ($R_{nl} = 200 \Omega$, $L_{nl} = 10 \text{ mH}$, $C_{nl} = 2200 \mu\text{F}$) with nominal filter parameters.

H Values	1	3.5	6.5	7	7.5	7.8
MPC-DOB (THD%)	NA	8.3	5.9	4.5	3.7	3.2
RC-DOB (THD%)	NA	6	5.1	4.8	4.4	7.7
RC-LOB (THD%)	NA	6.1	5.5	4.3	4.5	4.8

5.2. Experimental Results

A 5 KVA three-phase inverter with an output LC filter was used in the experiment. The DC link voltage for the inverter input was supplied by a three-phase diode rectifier. The control algorithm was implemented at 10 kHz sampling frequency on the TMS320F28377D DSP. A multi CAN converter and analyzer device was used to take the d-axis values from the DSP board to draw the d-axis figures in MATLAB. The three-phase voltages and THD values were measured using an oscilloscope and harmonic analyzer. The experimental setup of the system is given in Figure 8. The experiments were performed for different η values using MPC-DOB, RC-DOB, and RC-LOB under resistive, inductive, and nonlinear loads. For every η value, the observer gain matrices and the controller gain matrices were computed separately offline using MATLAB then implemented in the DSP.

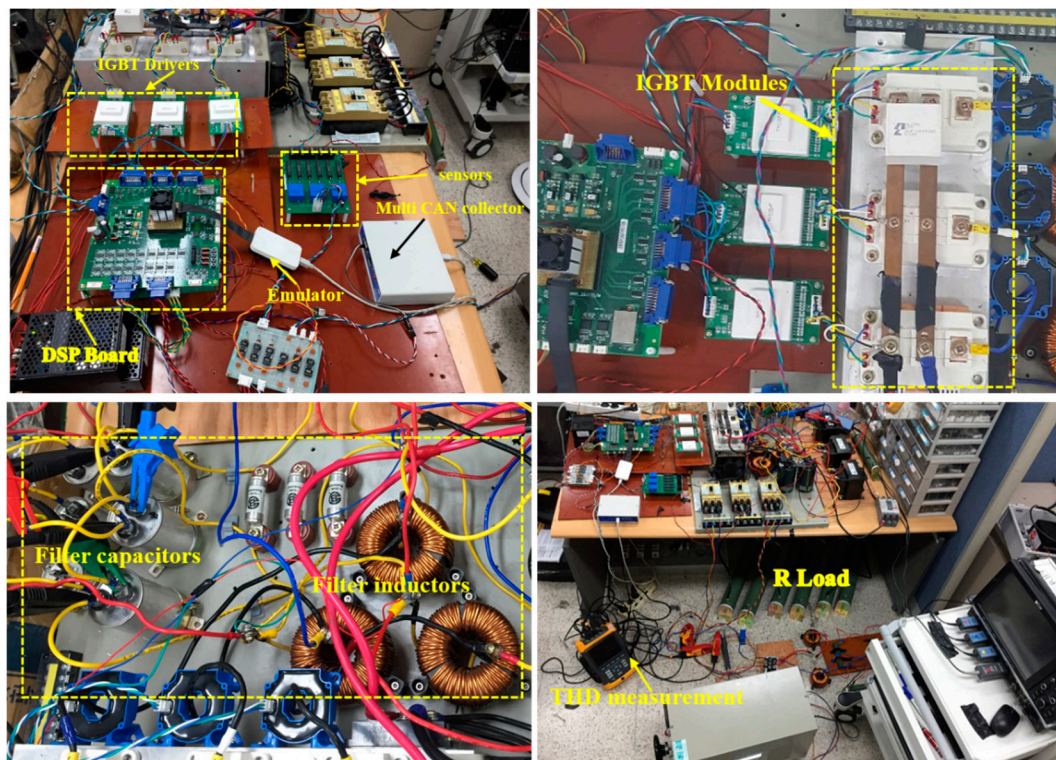


Figure 8. Experimental setup of the 5 kW three-phase inverter with output LC filter.

The comparative results were given in terms of the voltage THD in Tables 3–6 to show the performance of the proposed method under different load models for different uncertainty norm η .

A 10 Ω resistive load was connected to the output of the UPS, and 1.2% THD was obtained for $\eta = 7.8$ when MPC-DOB was used, as seen in Table 3. The THD values were high when RC-DOB and RC-LOB applied to the system under resistive load. The lowest THD was obtained 1.8% under the inductive load for $\eta = 7.8$ with MPC-DOB, as seen in Table 4. Although the performance of the other two methods was adequate, the proposed method (MPC-DOB) was better than that the other methods under inductive load. Table 5 shows the THD values under nonlinear load. For the larger model uncertainty ($\eta = 7.8$), lowest THD was obtained with the proposed method (3.1 % THD), RC-DOB could not stabilize the system, as seen in Table 5. The lowest THD was obtained for $\eta = 7.5$ with RC-DOB and RC-LOB. The control systems were evaluated under nonlinear load for different filter parameters ($L_f = 1.03$ mH, $C_f = 30$ μ F) to see the efficiencies in Table 6. The reasonable THD values were obtained with MPC-DOB and RC-DOB, RC-LOB could not stabilize the system with these values. Table 3-6 indicate that the design parameter η can be chosen as 7.8 for MPC-DOB and 7.5 for RC-DOB and RC-LOB in the experiment. Note that the THD differences between the simulation (Table 2) and experimental (Table 5) results can be caused by the measurement noise, variation in the filter parameters, cable losses, etc.

Table 3. THD values for different η under the resistive load ($R = 10 \Omega$).

H Values	1	3.5	6.5	7	7.5	7.8
MPC-DOB (THD%)	NA	1.9	1.5	1.4	1.3	1.2
RC-DOB (THD%)	NA	5.2	2.6	2.5	2.4	2.4
RC-LOB (THD%)	NA	4.2	3	2.5	2.3	2.3

Table 4. THD values for different η under the inductive load ($R_L = 10 \Omega$, $L_L = 10$ mH).

H Values	1	3.5	6.5	7	7.5	7.8
MPC-DOB (THD%)	NA	9.1	2.9	2.3	2.3	1.8
RC-DOB (THD%)	NA	6.1	2.6	2.4	2.4	2.4
RC-LOB (THD%)	NA	4.6	3.9	2.5	2.4	2.6

Table 5. THD values for different η under the nonlinear load ($R_{nl} = 200 \Omega$, $L_{nl} = 10$ mH, $C_{nl} = 2200$ μ F) with the nominal filter parameters.

η Values	1	3.5	6.5	7	7.5	7.8
MPC-DOB (THD%)	NA	10.2	7.7	5.4	4.1	3.1
RC-DOB (THD%)	NA	7.6	3.1	2.8	2.7	NA
RC-LOB (THD%)	NA	7.5	6	4.8	4.2	4.2

Table 6. THD values for different η under the nonlinear load ($R_{nl} = 200 \Omega$, $L_{nl} = 2.6$ mH, $C_{nl} = 2200$ μ F) with different filter parameters ($L_f = 1.03$ mH, $C_f = 30$ μ F).

η Values	4.5	5	6.5	7	7.5	7.8
MPC-DOB (THD%)	10	8.2	6.4	5.8	4.6	4.1
RC-DOB (THD%)	3.5	3.5	3.7	3.5	3.4	3.7

The performances of the steady-state control input $u_o(k)$ and the MPC-DOB control input $u^*(k)$ were compared in the experiment. Figure 9 shows the transient behavior of the resistive load current with $u_o(k)$ and $u(k)$ for $\eta = 7.8$. A fast and robust transient response is obtained with $u^*(k)$ similar to the simulation result given in Figure 6.

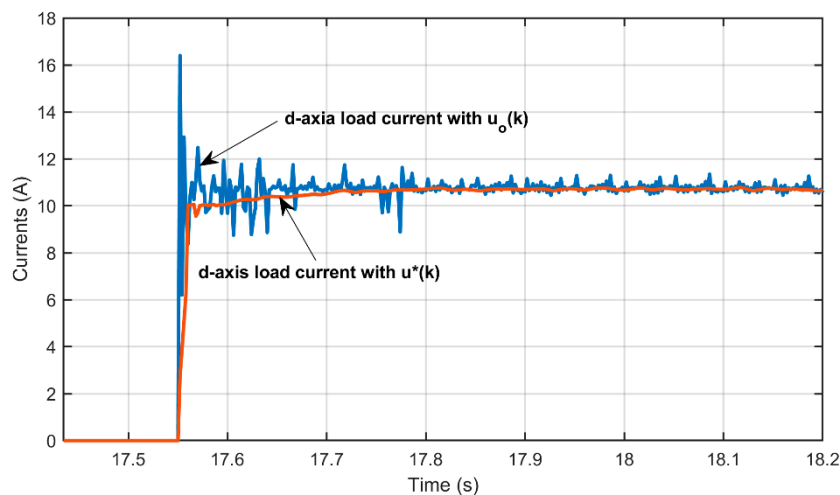


Figure 9. Transient response of the resistive load current with the control input MPC-DOB ($u(k)$) and the steady-state control input $u_o(k)$ for $\eta = 7.8$.

The transient response of the system was evaluated with MPC-DOB for different η values ($\eta = 4.5, 7.5$ and 7.8) under the step resistive load change. Figure 10 shows that a small η yields a fast transient, whereas a large η yields a slow transient. The d-axis voltage ripple in steady state comes from the measurement noise of the DSP board.

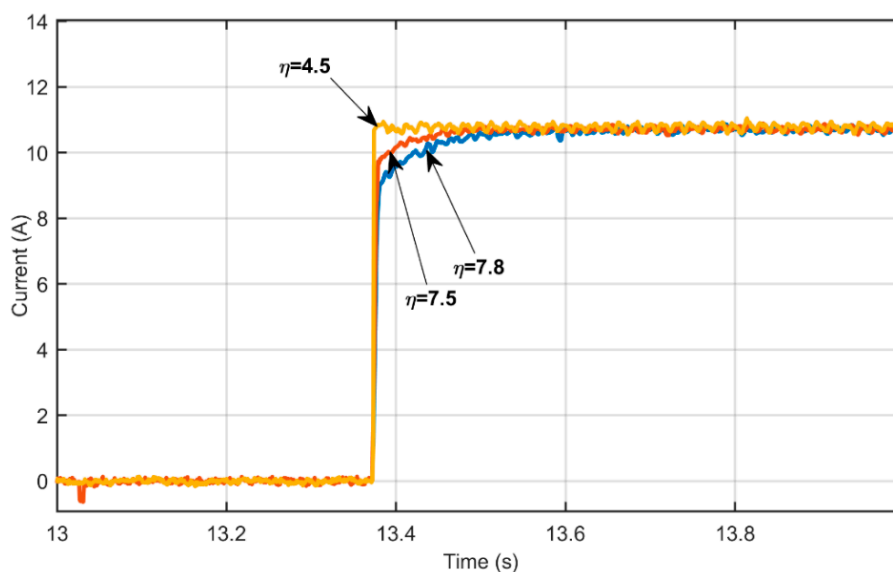


Figure 10. Experimental result of step load change from no load to R load step ($R = 10 \Omega$) for different η with MPC-DOB controller.

The steady state three-phase voltages are given in Figure 11 under resistive load ($R = 10 \Omega$). The uncertainty norm η was chosen as 7.8. It is showed that low voltage THD (in this experiment: $THD = 1.2\%$, acceptable value according to IEEE standards) could be obtained with MPC-DOB. Figure 12 shows the steady state three-phase voltages with MPC-DOB under nonlinear load ($R_{nl} = 200 \Omega, L_{nl} = 10 \text{ mH}, C_{nl} = 2200 \mu\text{F}, THD = 3.1\%$) for the design parameter $\eta = 7.8$. The transient performance of the method was evaluated under the load change from no load to nonlinear load. Figure 13 illustrates that a fast and smooth transient can be obtained with a small oscillation. The reason for the voltage rise during the load step could be a circuit breaker or the capacitor connected to the output of the diode rectifier.

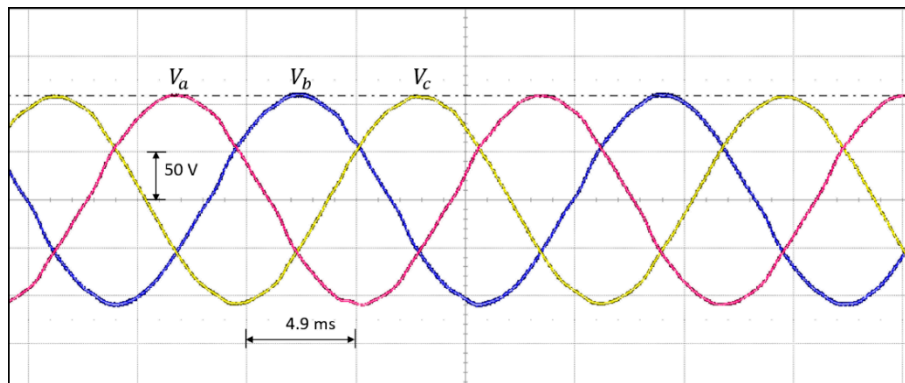


Figure 11. The steady state response of the three-phase output voltages with MPC-DOB under the resistive load ($\eta = 7.8$, $R = 10 \Omega$, $THD = 1.2\%$).

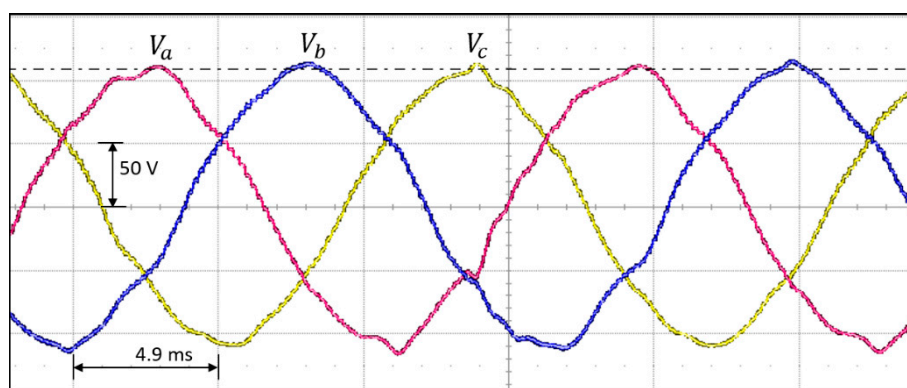


Figure 12. The steady state response of the three-phase output voltages with MPC-DOB under the nonlinear load ($\eta = 7.8$, $R_{nl} = 200 \Omega$, $L_{nl} = 10 \text{ mH}$, $C_{nl} = 2200 \mu\text{F}$, $THD = 3.1\%$).

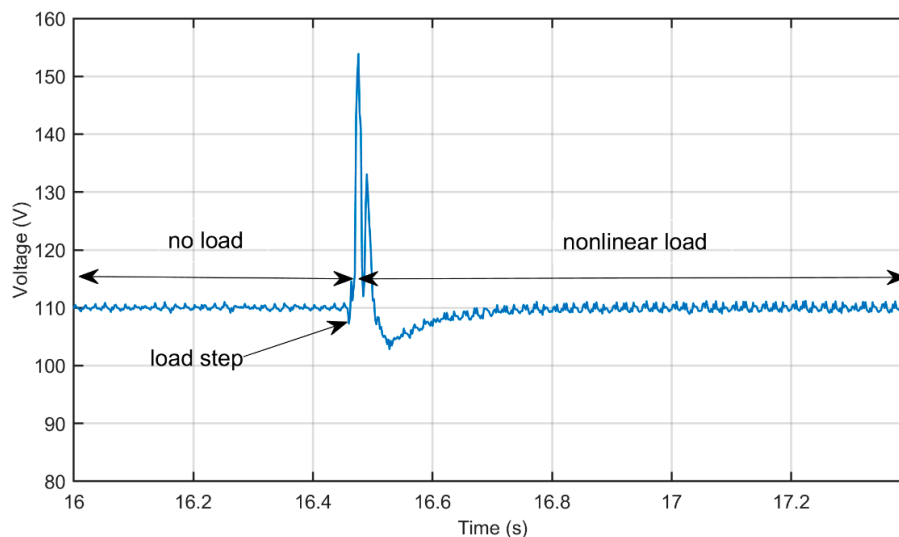


Figure 13. Transient response of the d-axis output voltage with MPC-DOB from no load to nonlinear load step ($THD = 3.1\%$, $\eta = 7.8$).

The transient response of the controllers was evaluated for the inductive and nonlinear loads, as seen in Figures 14 and 15, respectively. For a fair comparison, η was chosen as 7.5 for RC-DOB and RC-LOB and 7.8 for MPC-DOB based on the small THD values (chosen design parameters from Tables 3–6). For the inductive load, $R_L = 10 \Omega$, $L_L = 10 \text{ mH}$. and for the nonlinear load, $R_{nl} = 200 \Omega$, $L_{nl} = 10 \text{ mH}$, $C_{nl} = 2200 \mu\text{F}$ were chosen. MPC-DOB provided a faster transient response

in both load cases compared to the other two control methods. The simulation result given in Figure 7 showed a similar response with Figure 15.

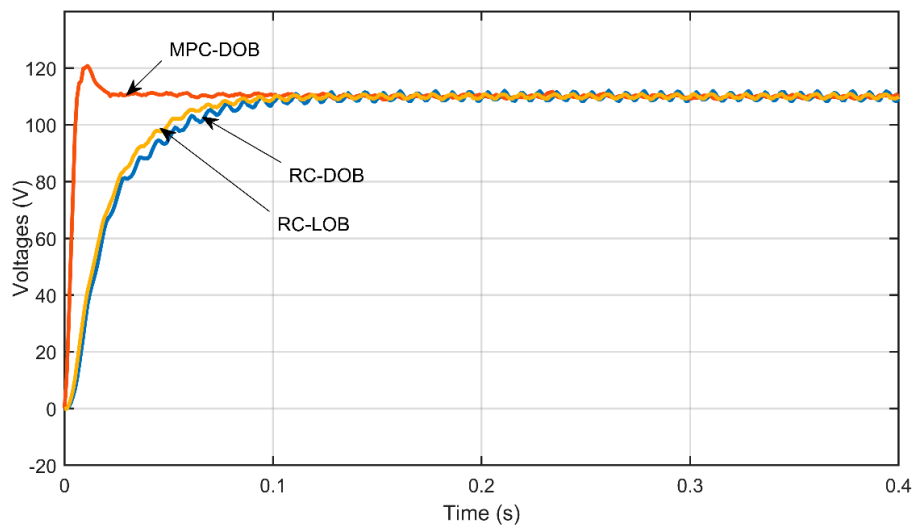


Figure 14. Transient response of MPC-DOB, RC-DOB, and RC-LOB under the inductive load.

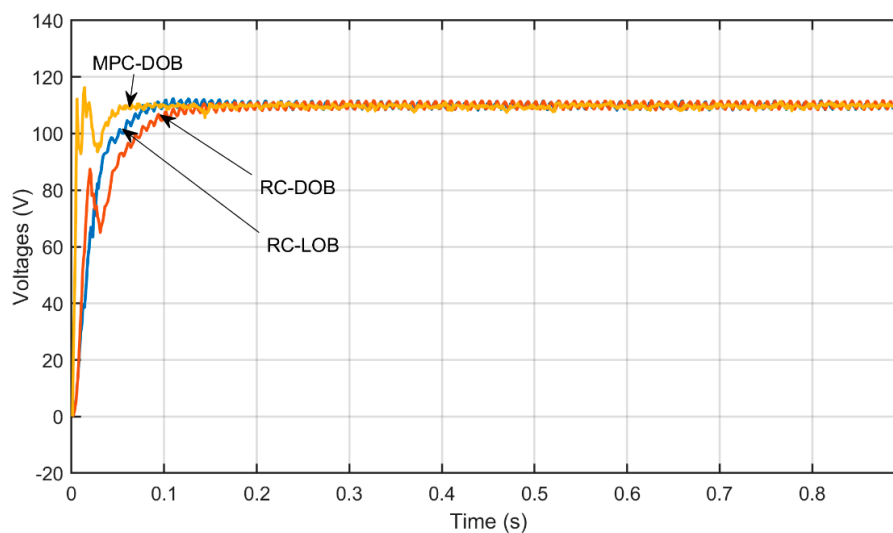


Figure 15. Transient response of MPC-DOB, RC-DOB, and RC-LOB under the nonlinear load.

The robustness of the proposed method was evaluated for different filter and nonlinear load parameters ($L_f = 1.03$ mH, $C_f = 30$ μ F, $C_{nl} = 2200$ μ F, $L_{nl} = 2.6$ mH, $R_{nl} = 200$ Ω). The capacitance of the filter was changed as 30 μ F, and the same inductance value was used 1.03 mH. The nominal filter parameters ($L_f = 1.03$ mH, $C_f = 50$ μ F) were used in the computation of the η values to evaluate the robustness of the proposed method under parameter change. Figure 16 shows that MPC-DOB and RC-DOB are robust against parameter change, and the transient response is faster with MP-DOB. RC-LOB was not included in the comparison, since it could not stabilize the system under the selected parameters. In Figures 14–16, we can see that MPC-DOB shows faster tracking performance than RC-DOB. The better tracking performance of MPC-DOB comes from minimizing the cost index of Equation (40), which penalizes the predicted tracking error.

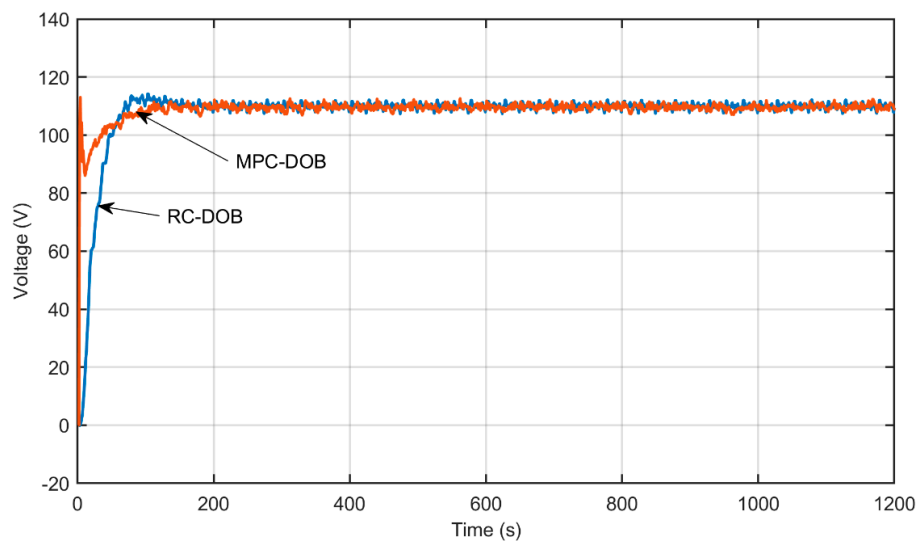


Figure 16. Transient response of MPC-DOB and RC-DOB under the nonlinear load with different filter parameters ($\eta = 7.5$).

6. Conclusions

This study proposed a robust disturbance observer-based CCS-MPC to control the output voltage of a three-phase inverter with an output LC filter for UPS applications. The lumped disturbances (parameter uncertainties and the disturbance effect of the load current) were considered in the controller design to obtain a robust performance. A discrete time robust disturbance observer was proposed to compensate for the effect of the lumped disturbances. An LMI matrix was defined to obtain an optimal observer gain matrix, and an optimization problem was given for the computation of the gain matrix taken into account the model uncertainties. A two-step ahead prediction was used to compensate for the time delay caused by the computation and the SVPWM.

The use of the proposed DOB with CCS-MPC enabled the precise prediction of the system states in the steady state and the offset-free tracking control of a UPS system. The DOB can compensate for the effect of the model uncertainties and the disturbance load current without any additional observer. The efficacy of the proposed method was proven through simulation and experimental studies. The comparative results were given for MPC-DOB, RC-DOB, and RC-LOB. The proposed method was applied a 5-KVA three-phase inverter with an output LC filter using TMS320F28377D DSP at 10 kHz sampling frequency. The experimental results show that the proposed DOB with CCS-MPC yields a good voltage tracking performance with proper calculation of the DOB gain matrix. The use of the proposed method improved transient performance during the load change in a UPS system. The experimental results show that the method can be used with the chosen design parameter in the practical applications.

Author Contributions: Conceptualization, Y.I.L.; methodology, Y.I.L. and Y.D; software, Y.D.; validation, Y.D., M.C. and K.L.; formal analysis, Y.D.; investigation, Y.D; resources, Y.D., M.C and K.L.; data curation, Y.D., M.C. and K.L.; writing—original draft preparation, Y.D.; writing—review and editing, Y.I.L. and Y.D.; visualization, Y.D.; supervision, Y.I.L.; project administration, Y.I.L.; funding acquisition, Y.I.L.

Funding: National Research Foundation of Korea: NRF-2019R1A6A1A03032119, The Scientific and Research Council of Turkey: 1059B141601385.

Conflicts of Interest: The authors declare no conflict of interest.

Abbreviations

FCS-MPC	finite control set model predictive control
CCS-MPC	continuous control set model predictive control
DOB	disturbance observer
MPC-DOB	model predictive control with the disturbance observer
RC	robust control
RC-DOB	robust control with the disturbance observer
RC-LOB	robust control with Luenberger type observer
UPS	uninterruptible power supply
THD	total harmonic distortion
LMI	linear matrix inequality
SVPWM	space vector pulse width modulation
KVA	kilo volt ampere
LC	inductor-capacitor
DSP	digital signal processor

Notations

R	nominal value of resistor
L_f	nominal value of filter inductor
C_f	nominal values of filter capacitor
R_1	lower value of resistor
R_2	upper value of resistor
L_1	lower value of filter inductor
L_2	upper value of filter inductor
C_1	lower value of filter capacitor
C_2	upper value of filter capacitor
u	control input
u_0	Steady-state control input
u^*	optimal control input
U_h	switching function
x	system state
x^*	reference system state
$x(k+1 k)$	predicted system state
A_n	nominal system matrix
B_n	nominal input matrix
W_n	nominal disturbance matrix
\hat{A}	uncertain system matrix
\hat{B}	uncertain input matrix
d_L	actual lumped disturbance
\hat{d}_L	estimated lumped disturbance
L	disturbance observer gain matrix
J	cost function
\mathcal{P}	polytopic uncertainty class
p	number of uncertain parameter
γ	increment of parameter
η	uncertainty norm
P_{cl}	positive definite matrix for the close loop system
\hat{Q}	positive definite matrix for the uncertain system
P_{cost}	weight matrix for the cost function
P_{obv}	positive definite matrix for the observer system
G	positive definite matrix for the observer system
G_0	positive definite matrix for the observer system
ε	design parameter for the optimization problem
\bar{R}	weight matrix for control input
K	state feedback gain
Z	integrator gain

References

1. Mattavelli, P. An improved deadbeat control for UPS using disturbance observers. *IEEE Trans. Ind. Electron.* **2005**, *52*, 206–212. [[CrossRef](#)]
2. Kukrer, O.; Komurcugil, H. Deadbeat control method for single-phase UPS inverters with compensation of computation delay. *IEEE Proceed. Elect. Pow. Appl.* **1999**, *146*, 123–128. [[CrossRef](#)]
3. Escobar, G.; Valdez, A.A.; Leyva-Ramos, J.; Mattavelli, P. Repetitive-Based Controller for a UPS Inverter to Compensate Unbalance and Harmonic Distortion. *IEEE Trans. Ind. Electron.* **2007**, *54*, 504–510. [[CrossRef](#)]
4. Zhang, K.; Kang, Y.; Xiong, J.; Chen, J. Direct repetitive control of SPWM inverter for UPS purpose. *IEEE Trans. Power Electron.* **2003**, *18*, 784–792. [[CrossRef](#)]
5. Ito, Y.; Kawauchi, S. Microprocessor based robust digital control for UPS with three-phase PWM inverter. *IEEE Trans. Power Electron.* **1995**, *10*, 196–204. [[CrossRef](#)]
6. Valderrama, G.E.; Stankovic, A.M.; Mattavelli, P. Dissipativity-based adaptive and robust control of UPS in unbalanced operation. *IEEE Trans. Power Electron.* **2003**, *18*, 1056–1062. [[CrossRef](#)]
7. Lim, J.S.; Park, C.; Han, J.; Lee, Y.I. Robust Tracking Control of a Three-Phase DC-AC Inverter for UPS Applications. *IEEE Trans. Ind. Electron.* **2014**, *61*, 4142–4151. [[CrossRef](#)]
8. Willmann, G.; Coutinho, D.F.; Pereira, L.F.A.; Libano, F.B. Multiple-Loop H-Infinity Control Design for Uninterruptible Power Supplies. *IEEE Trans. Ind. Electron.* **2007**, *54*, 1591–1602. [[CrossRef](#)]
9. Rodriguez, J.; Kazmierkowski, M.P.; Espiniza, J.R.; Zanchetta, P.; Abu-Rub, H.; Young, H.A.; Rojas, C.A. State of the Art of Finite Control Set Model Predictive Control in Power Electronics. *IEEE Trans. Ind. Inform.* **2013**, *9*, 1003–1016. [[CrossRef](#)]
10. Parvez, A.M.S.; Mekhilef, N.; Lin, T.; Akagi, H. Modified Model Predictive Control of a Bidirectional AC-DC Converter Based on Lyapunov Function for Energy Storage Systems. *IEEE Trans. Ind. Electron.* **2016**, *63*, 704–715. [[CrossRef](#)]
11. Young, H.A.; Perez, M.A.; Rodriguez, J. Analysis of Finite-Control-Set Model Predictive Current Control with Model Parameter Mismatch in a Three-Phase Inverter. *IEEE Trans. Ind. Electron.* **2016**, *63*, 3100–3107. [[CrossRef](#)]
12. Wang, J.; Wang, F.; Zhang, Z.; Li, S.J.; Rodríguez, J. Design and Implementation of Disturbance Compensation-Based Enhanced Robust Finite Control Set Predictive Torque Control for Induction Motor Systems. *IEEE Trans. Ind. Inform.* **2017**, *13*, 2645–2656. [[CrossRef](#)]
13. Xia, C.; Wang, M.; Song, Z.; Liu, T. Robust Model Predictive Current Control of Three-Phase Voltage Source PWM Rectifier with Online Disturbance Observation. *IEEE Trans. Ind. Inform.* **2012**, *8*, 459–471. [[CrossRef](#)]
14. Nguyen, H.T.; Kim, E.; Kim, I.; Choi, H.H.; Jung, J. Model Predictive Control with Modulated Optimal Vector for a Three-Phase Inverter with an LC Filter. *IEEE Trans. Power Electron.* **2018**, *33*, 2690–2703. [[CrossRef](#)]
15. Kim, S.K.; Park, C.R.; Yoon, T.W.; Lee, Y.I. Disturbance-observer-based model predictive control for output voltage regulation of three-phase inverter for uninterruptible-power-supply applications. *Eur. J. Control.* **2015**, *23*, 71–83. [[CrossRef](#)]
16. Lee, K.; Lee, J.; Back, J.; Lee, Y.I. A Robust Emulation of Mechanical Loads Using a Disturbance-Observer. *Energies* **2019**, *12*, 2236. [[CrossRef](#)]
17. Han, S.I. Tracking Error Constrained Super-twisting Dynamic Surface Control of Partially Known Nonlinear Systems with a Super-twisting Nonlinear Disturbance Observer. *IJCAS* **2019**, *17*, 867–879. [[CrossRef](#)]
18. Lee, Y.S.; Kim, D.S.; Kim, S.K. Disturbance Observer-based Proportional-type Position Tracking Controller for DC Motor. *IJCAS* **2018**, *16*, 2169–2176. [[CrossRef](#)]
19. Chen, K.Y. Robust Optimal Adaptive Sliding Mode Control with the Disturbance Observer for a Manipulator Robot System. *IJCAS* **2018**, *16*, 1701–1715. [[CrossRef](#)]
20. Choeung, C.; Park, S.H.; Koh, B.K.; Lee, Y.I. Robust Tracking Control of a Three-Phase DC-AC Inverter for UPS Application under Unbalanced Load Conditions. In Proceedings of the IFAC Workshop on Control of Transmission and Distribution Smart Grids, Prague, Czech Republic, 11–13 October 2016.
21. Rodríguez, J.; Cortes, P. *Predictive Control of Power Converters and Electrical Drives*, 1st ed.; Wiley-IEEE Press: New York, NY, USA, 2012; pp. 7–39.

22. Wang, L.; Chai, S.; Yoo, D.; Gan, L.; Ng, K. *PID and Predictive Control of Electrical Drives and Power Converters Using MATLAB/Simulink*, 1st ed.; Wiley-IEEE Press: Singapore, 2014.
23. Boyd, S.P.; Ghaoui, L.E.; Feron, E.; Balakrishnan, V. *Linear Matrix Inequalities in System and Control Theory*, 1st ed.; SIAM: Philadelphia, PA, USA, 1994; pp. 3–155.



© 2019 by the authors. Licensee MDPI, Basel, Switzerland. This article is an open access article distributed under the terms and conditions of the Creative Commons Attribution (CC BY) license (<http://creativecommons.org/licenses/by/4.0/>).